Targetome

ORIGINAL ARTICLE

Open Access

https://doi.org/10.48130/targetome-0026-0012

Targetome **2026**, 2(2): e014

Crocin II alleviates metabolic dysfunction-associated steatotic liver disease by enhancing autophagic degradation of ANGPTL8

Rongtian Zhang[#], Kongdong Li[#], Ziting Zhao, Xintong Jiang, Rumeng Zhang, Chang Liu[*], Wenxiang Zhang[*] and Siyu Chen[*]

State Key Laboratory of Natural Medicines, School of Life Science and Technology, China Pharmaceutical University, Nanjing 211198, China

[#] Authors contributed equally: Rongtian Zhang, Kongdong Li

[*] Correspondence: changliu@cpu.edu.cn (Liu C); wenxiangzhang@cpu.edu.cn (Zhang W); siyuchen@cpu.edu.cn (Chen S)

Abstract

Metabolic dysfunction-associated steatotic liver disease (MASLD) has emerged as a severe public health crisis, affecting more than a quarter of the adult population. ANGPTL8 is a potential therapeutic target for MASLD owing to its dual roles in lipid and inflammatory regulation. However, current targeting strategies are inadequate, particularly in the realm of natural compound-driven protein degradation inducers. In this study, we utilize molecular docking analysis, a cellular thermal shift assay, a drug affinity responsive target stability assay, and a surface plasmon resonance assay to identify Crocin II as a potential candidate for targeting ANGPTL8. We demonstrate that Crocin II can facilitate the degradation of ANGPTL8 protein via the autophagosome-lysosome pathway. Pharmacodynamically, Crocin II ameliorates HFD-induced MASLD by targeting ANGPTL8, with no overt adverse effects in murine kidneys, hearts, and spleens. In conclusion, our study demonstrates that Crocin II has a favorable therapeutic effect on MASLD by targeting ANGPTL8 and promoting its protein degradation, indicating that Crocin II is a promising candidate for MASLD therapy.

Citation: Zhang R, Li K, Zhao Z, Jiang X, Zhang R, et al. 2026. Crocin II alleviates metabolic dysfunction-associated steatotic liver disease by enhancing autophagic degradation of ANGPTL8. *Targetome* 2(2): e014 https://doi.org/10.48130/targetome-0026-0012

Introduction

Metabolic dysfunction-associated steatotic liver disease (MASLD) has emerged as a rapidly escalating yet underappreciated global public health crisis[1]. Affecting over one-quarter of the adult population, its worldwide prevalence in adults is 30%[2]. Strongly intertwined with metabolic risk factors, including obesity, hypertension, dyslipidemia and type 2 diabetes, MASLD has been linked to an increased risk of morbidity and mortality from chronic kidney disease (CKD), cardiovascular disease (CVD), and multiple cancer types[3,4]. Over the past decade, the incidence of liver transplantation for MASLD-related cirrhosis has surged tenfold, with Bayesian modeling forecasting a striking 55.7% global prevalence by 2040[5,6]. Liver-related mortality in MASLD patients is 1.75 per 1,000 person-years, with mortality rates rising nearly exponentially as fibrosis advances[7]. By 2030, a disproportionate increase in advanced hepatic fibrosis (stages F3–F4) is expected, alongside a 2- to 3-fold rise in liver cirrhosis, hepatocellular carcinoma (HCC), and cirrhosis-related mortality[8,9]. Although numerous intervention targets, such as the Farnesoid X Receptor (FXR), and small-molecule drugs, including obeticholic acid, have been identified, their clinical efficacy has been suboptimal[10,11]. Thus, further research into the molecular pathogenesis of MASLD and the development of tailored, safe therapeutic strategies are now urgent priorities.

Among the Angiopoietin-like protein (ANGPTL) protein family, ANGPTL8 is characterized by the absence of several structural consensuses typically observed in other ANGPTL family members. Its structure lacks an N-terminal coiled-coil domain, a C-terminal fibrinogen-like domain, and canonical glycosylation patterns[12]. ANGPTL8 is highly expressed in the liver and brown adipose tissue in mice, but restricted to the liver in humans, supporting that circulating ANGPTL8 is a liver-derived factor[13]. Functionally, ANGPTL8 promotes the cleavage of ANGPTL3 to regulate the activity of lipoprotein lipase (LPL) and lipid metabolism[12,14]. Furthermore, ANGPTL8 binds to the paired immunoglobulin-like receptor B (PIRB) on the hepatocyte membrane. This specific binding integrates food-induced resetting of the hepatic circadian clock and lipid homeostasis in mice. Hence, ANGPTL8 serves as a potential novel *Zeitgeber* for peripheral clocks and lipid metabolism in the liver[15]. Despite the disruption of lipid metabolism, chronic inflammation contributes to the progression of MASLD[16]. Concurrently, plasma ANGPTL8 levels positively correlate with increased systemic inflammation in MASLD, while TNF-α and LPS are known stimuli to trigger hepatic ANGPTL8 expression[17]. *Angptl8* deficiency ameliorates LPS-induced liver injury by reprogramming hepatocyte lipid metabolism and macrophage glycogen metabolism[18,19]. Meanwhile, ANGPTL8 triggers macrophage recruitment during non-alcoholic steatohepatitis progression *via* its receptor LILRB2/PIRB[20,21]. Hence, ANGPTL8 potentially holds the promise to serve as a valuable target for MASLD therapy.

To achieve therapeutic efficacy for MASLD by targeting *Angptl8*, antisense oligonucleotides (ASOs) have been designed to knock down the expression of *Angptl8*. Such a nucleotide-based gene knockdown effectively prevents diet-induced MASLD and hepatic insulin resistance in rodent models[22]. Additionally, a monoclonal anti-ANGPTL8 antibody was generated to neutralize circulating ANGPTL8 in mice. This antibody sufficiently enhances energy expenditure, reduces body weight, and disrupts food-entrained resetting of the hepatic circadian clock and metabolic rhythmicity in mice[23]. Although both targeting strategies effectively abrogate ANGPTL8 expression and function, their clinical potential is still debated. For nucleotide-based ASOs, the instability of nucleic acids and the lack of safe drug delivery systems limit their clinical translation[24]. Meanwhile, the short half-life and high production costs of the monoclonal antibody approach hinder its clinical application[25]. Compared with these novel biological drugs, plant-derived natural chemical monomers exert inherent advantages, such as abundant resources, fewer adverse effects, and low costs. Thus, studies aiming

to identify natural compounds specifically targeting ANGPTL8 may provide promising therapeutics for MASLD.

In our study, we focused on saffron, a highly valued agricultural product. The Jingzhu Bencao (an ancient herbal text) records: 'Saffron alleviates all liver disorders'. Previous studies demonstrate that saffron extract reduces the LDL/HDL ratio and serum lipid levels in rats suffering from coronary atherosclerosis[26]. Taking advantage of network pharmacology, MOE analyses, CETSA, DARTS, and SPR assays, we identified Crocin II as a potential candidate targeting ANGPTL8. Moreover, Crocin II promoted ANGPTL8 protein degradation via the autophagosome-lysosome pathway. Pharmacodynamically, Crocin II ameliorated the hepatic steatosis, reprogrammed the hepatic lipidomic landscape, and exhibited *in vivo* organ safety in HFD-induced MASLD mice. This discovery positions Crocin II as a promising agent for MASLD patients with fatty liver diseases and hyperlipidemia.

Materials and methods

Drug screening

A small-molecule library of natural compounds containing 70 chemical monomers was constructed based on saffron through network pharmacology, and the 3D structural files of the compounds were obtained from PubChem. The 3D structure of the ANGPTL8 protein was downloaded from the PDB database for subsequent molecular docking. Ligand design and molecular docking were performed using the Molecular Operating Environment software v2024.06 (MOE). Pose values of 30 and 5 were selected for docking. The *S*-score was used to evaluate ligand-protein interactions. Lower *S*-scores indicated stronger interactions with human ANGPTL8.

Cell culture

Mouse primary hepatocytes (PHs) were isolated from C57BL/6J wild-type (WT) or *Angptl8* knockout (*Angptl8*$^{-/-}$) mice (GemPharmatech Co., Ltd, Nanjing, China) using the perfusion method with collagenase IV (Sigma-Aldrich, St. Louis, MO, USA) as previously described[27]. Mouse PHs were cultured in a humidified atmosphere containing 5% CO_2 at 37 °C.

mRNA and protein expression analyses

Total RNA was isolated and analyzed as described previously[19]. The primers for mouse 36B4 were used for normalization of gene expression. A complete list of PCR primers is presented in Supplementary Table S1. For protein expression analysis, tissues were homogenized, and the cells were lysed in RIPA buffer. The protein concentration was quantified with a BCA protein quantification kit (Bio-Rad, Hercules, CA, USA). Protein levels were assessed by Western blot analysis. The detailed procedure has been described previously[28]. NIH ImageJ 1.32j software was used for the quantitative analysis of blots. The antibodies against β-Actin (Cat. No. AC038, 1 : 1,000 dilution) and LC3 I/II (Cat. No. A5618, 1 : 1,000 dilution) were purchased from Abclonal (Nanjing, Jiangsu, China), ANGPTL8 (Cat. No. PA5-38043, 1 : 1,000 dilution) was purchased from Thermo Fisher (Waltham, MA, USA), and P62 (Cat. No. AP6006, 1 : 1,000 dilution) was obtained from Bioworld (Nanjing, Jiangsu, China).

Cellular thermal shift assay (CETSA)

Mouse PHs were pretreated with 100 μmol·L^{-1} Crocin I or Crocin II for 3 h, then the cells were equally divided into six groups and heated at different temperatures (40–65 °C, 5 °C intervals) for 3 min. Subsequently, mouse PHs were lysed via the liquid nitrogen freeze-thaw method to prepare total proteins for Western blot analysis.

Drug affinity responsive target stability (DARTS) assay

Total cellular proteins were isolated via RIPA lysis buffer. Cell lysates were incubated with indicated doses of DMSO, Crocin I or Crocin II at 25 °C for 2 h, then pronase was added to the experimental groups and incubated for 30 min at 37 °C. The protein levels of ANGPTL8 were analyzed in all samples by Western blot.

Surface plasmon resonance (SPR) assay

PBSP buffer was filtered through a 0.22 μm membrane. The human ANGPTL8 protein was diluted to 10 μg·mL^{-1} with 10 mmol·L^{-1} sodium acetate (pH 4.5). The CM5 chip surface was activated with EDC (400 mmol·L^{-1}) and NHS (100 mmol·L^{-1}) at a flow rate of 10 μL·min^{-1} for 480 s. Subsequently, the ANGPTL8 protein was injected into the experimental channel at a flow rate of 10 μL·min^{-1}, respectively, with a fixation volume of approximately 10,000 RU. The chip was closed with 1 mol·L^{-1} ethanolamine at a flow rate of 10 μL·min^{-1} for 480 s. Gradient concentrations of Crocin I or Crocin II were injected into the channels to evaluate the binding affinity. Multi-cycle kinetic analysis was performed on the analytes, with raw experimental data processed by Biacore S200 Evaluation Software and curve fitting conducted via a 1 : 1 Langmuir kinetic binding model.

Molecular dynamics

The protein structure of human ANGPTL8 was obtained from the PDB database. The 3D structure of Crocin II was downloaded from PubChem. Molecular dynamics (MD) simulations were assessed by using Gromacs2023.3, while Amber ff14SB force field parameters were used for the proteins[29,30]. A small molecule force field file was generated using Sobtop software with the GAFF force field. Files for the protein and small molecule ligand were combined to construct the simulation system for the complex, and the system was prepared by adding TIP3P water molecules and neutralized with 0.15 mol·L^{-1} NaCl. Following system minimization and 500 ps of NVT and NPT equilibration simulations, a 200 ns production simulation was carried out in an isothermal-isobaric ensemble at 310.15 K and 1 bar, with trajectory coordinates logged every 10 ps.

Monomeric cherry (mCherry)-enhanced green fluorescent protein (eGFP)–LC3 adenovirus assay

mCherry–eGFP–LC3 adenoviruses were obtained from HanBio Technology Co., Ltd (Shanghai, China). The adenoviruses were designed to evaluate the autophagy in cells[31]. Mouse PHs were infected with the adenoviruses at an MOI of 100 following the manufacturer's recommended protocols. After treatment, LC3 puncta were examined by a Nikon fluorescence microscope (400× magnification, ECLIPSE, Ts2R-FL, Tokyo, Japan).

Plasmids transfection

The plasmids encoding the mouse *Angptl8* CDS were synthesized by Bioworld (Nanjing, Jiangsu, China) and were transiently transfected into mouse PHs using the Lipofectamine 3000 reagent (Thermo Fisher, Shanghai, China) according to the manufacturer's guidelines. Twenty four hours later, cells were pretreated with 100 μmol·L^{-1} Crocin II for 2 h, then exposed to 0.4 mmol·L^{-1} FFAs and 100 μmol·L^{-1} Crocin II for another 24 h.

Cell viability

A CCK-8 cytotoxicity assay was performed to evaluate the toxic impacts of Crocin II on the cell viability of mouse PHs. In brief, cells were seeded at a density of 10^4 cells per well in a 96-well plate and cultured at 37 °C overnight. The medium was replaced with 100 μL of fresh medium supplemented with either 0.1% dimethyl sulfoxide (DMSO) or Crocin II at indicated concentrations for an additional 24 h. After that, 10 μL CCK-8 reagent (Abbkine, Wuhan, China) was added to each well for 2 h. The absorbance value at a wavelength of 450 nm was detected using a microplate reader (TECAN, SPARK, Salzburg, Austria).

Cellular ORO and Nile Red staining

Oil Red O (ORO) and Nile Red were obtained from Sigma-Aldrich (St. Louis, MO, USA). For ORO staining, mouse PHs were fixed with 4% paraformaldehyde (PFA) for 30 min, followed by 0.5% (*W/V*) ORO staining for 15 min. All the stained sections were observed by a Nikon light microscope (400× magnification, ECLIPSE, Ts2R-FL, Tokyo, Japan). For Nile Red staining, mouse PHs were similarly fixed and cotreated with 0.1 mg·mL^{-1} Nile Red and 2 μg·mL^{-1} DAPI for 5 min. After washing, samples were photographed with a Nikon fluorescence microscope (400× magnification, ECLIPSE, Ts2R-FL, Tokyo, Japan).

Measurement of intracellular triglyceride

Mouse PHs were lysed by 0.1% Triton X-100 (Solarbio, Beijing, China) and cell lysates were used to assess the intracellular triglyceride (TG) content using a commercial kit following the manufacturer's instructions (Jiancheng, Nanjing, China).

Animals

Age-matched C57BL/6J male mice were purchased from GemPharmatech (Nanjing, China) and were maintained in a 12 h light/dark cycle in standard conditions (temperature 21–23 °C, humidity 40%–60%). To establish the MASLD model, 10-week-old male mice were fed on a high-fat diet (HFD) containing 60% kcal fat (Research Diet, New Brunswick, NJ, USA) or a normal standard diet (ND) for 10 weeks. To evaluate the beneficial effects of Crocin II on MASLD pathology, mice were divided randomly into five groups: ND + Saline group, HFD + Saline group, HFD + 5 mg·kg^{-1} Crocin II (low dose, L) group, HFD + 10 mg·kg^{-1} Crocin II (medium dose, M) group, and HFD + 20 mg·kg^{-1} Crocin II (high dose, H) group (n = 6 per group). The Crocin II (purity > 97%) was purchased from Biopurify Phytochemicals (Chengdu, China). Mice of Crocin II-treated groups received daily intraperitoneally (*i.p.*) administrated Crocin II (5, 10, and 20 mg·kg^{-1} body weight, respectively). Food intake and body weight were monitored weekly throughout the experiment. All mice were euthanized, and the liver tissues were harvested after 10 weeks HFD feeding.

Tolerance tests

For the glucose tolerance test (GTT), mice were fasted for 16 h followed by *i.p.* injection with glucose at a dose of 1 g·kg^{-1} body weight. For the insulin tolerance test (ITT), mice were fasted for 6 h and *i.p.* injected with indicated doses of insulin (0.75 U·kg^{-1} body weight for ND-fed mice, and 2 U·kg^{-1} body weight for HFD-fed mice). Blood glucose levels were determined at specific time points post-injection with a glucose monitor (Bayer, Leverkusen, Germany).

Serological analysis

Serum concentrations of alanine aminotransferase (ALT), aspartate aminotransferase (AST), TG, total cholesterol (TC), LDL-cholesterol (LDL-C), HDL-cholesterol (HDL-C), blood urea nitrogen (BUN), creatinine, atrial natriuretic peptide (ANP), and B-type natriuretic peptide (BNP) were evaluated using commercial kits (Jiancheng, Nanjing, Jiangsu, China) according to the manufacturers' instructions.

H&E and ORO staining

Fresh liver tissues were fixed in a 4% PFA for 24 h, processed for paraffin embedding. Paraffin-embedded samples were sectioned at a thickness of 5 μm and subjected to hematoxylin and eosin (H&E) staining. ORO staining was performed on frozen liver sections (6 μm thick) using a 0.5% (*W/V*) ORO solution for 15 min. Slides were digitized with a NanoZoomer 2.0-RS scanner (Hamamatsu, Japan) and analyzed using the NDP view 2 software (Hamamatsu, Japan).

Liver TG and TC analyses

For liver lipid measurements, 50 mg liver samples were homogenized, and TG and TC contents were measured using commercial kits (Jiancheng, Nanjing, China) according to the manufacturer's instructions.

Liver lipidomics

The lipidome in the liver was performed at Beijing Novogene Biotech Co., Ltd (Beijing, China) as previously described[32]. Briefly, liver lipids were extracted using a Chloroform: methanol-based method. Liver lipid extracts were analyzed *via* a Vanquish UHPLC (Thermo Fisher, Waltham, MA, USA) coupled to a Q Exactive HF-X mass spectrometer (Thermo Fisher, Waltham, MA, USA). Lipid annotation was achieved by matching MS/MS fragment patterns, with accurate mass information retrieved from the Lipid Maps database.

Statistical analysis

All statistical analyses were performed using GraphPad Prism10.3.0 (San Diego, CA, USA). The data was presented as mean ± standard deviation (SD). One-way ANOVA followed by Bonferroni's post hoc test were performed to analyze the data. A P-value < 0.05 was considered statistically significant.

Results

Compound screenings identify Crocin II as a potential drug targeting ANGPTL8

To identify novel natural compounds targeting human ANGPTL8, we performed a comprehensive screen of saffron-derived constituents using the TCMSP system[33], identifying 70 small-molecule compounds (Fig. 1a). Subsequent molecular docking analyses of human and mouse ANGPTL8 against these candidates revealed that Crocin I and Crocin II exhibited high binding affinity (Fig. 1b–e; Supplementary Tables S2 and S3). To further evaluate the binding capacity of these candidate compounds to ANGPTL8, we assessed their effects on ANGPTL8 protein thermal stability using a CETSA assay. As shown in Fig. 1 and Supplementary Fig. S1a, CETSA confirmed the binding of both Crocin I and II to ANGPTL8. The results indicated that both Crocin I and II binding promoted ANGPTL8 degradation at elevated temperatures, while Crocin II exhibited a stronger ability to promote ANGPTL8 degradation. The

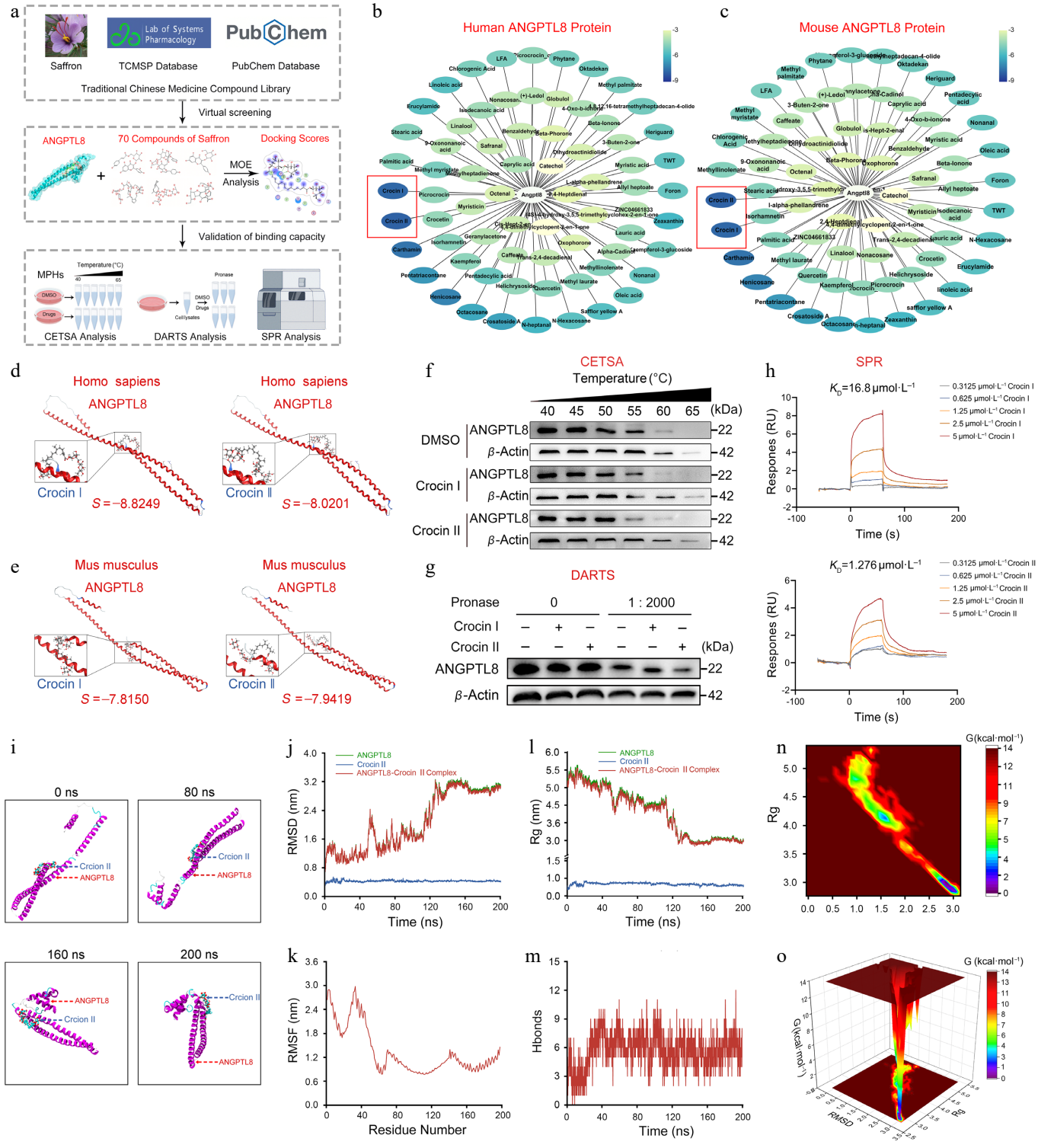

Fig. 1 Compound screenings identify Crocin II as a potential drug targeting ANGPTL8. (a) Workflow for screening small-molecule compounds targeting ANGPTL8. (b) MOE analysis of binding potentials of natural small-molecule compounds on human ANGPTL8. (c) MOE analysis of binding potentials of natural small-molecule compounds on mouse ANGPTL8. (d) The binding pattern of human ANGPTL8 with Crocin I and Crocin II. (e) The binding pattern of mouse ANGPTL8 with Crocin I and Crocin II. (f) Mouse PHs were exposed to DMSO, 100 μmol·L^{-1} Crocin I or Crocin II for 3 h, then subjected to CETSA analysis. Western blot analysis for the protein levels of ANGPTL8. (g) Mouse PHs lysates were incubated with DMSO, 100 μmol·L^{-1} Crocin I or Crocin II for 2 h at 25 °C, followed by digestion with pronase for 30 min at 37 °C. Western blot analysis for the protein levels of ANGPTL8. (h) The direct combination of ANGPTL8 with Crocin I or Crocin II was evaluated using SPR. (i) Representative snapshots of molecular dynamics processes. (j) RMSD curves. (k) RMSF curve. (l) Rg curves. (m) Fluctuation curve of the number of hydrogen bonds. (n) The two-dimensional mapping of the free energy landscape. (o) The three-dimensional mapping of the free energy landscape. Data are presented as the mean ± SEM, n = 3.

results from DARTS confirmed that the interaction of Crocin II with ANGPTL8 triggered its protein degradation (Fig. 1g and Supplementary Fig. S1b). More importantly, the SPR assay revealed the binding affinity between Crocin I/II and ANGPTL8, respectively, with dissociation constants (K_D) of 16.8 μmol·L^{-1} for Crocin I and 1.276 μmol·L^{-1} for Crocin II (Fig. 1h). It is noteworthy that Crocin II demonstrates a markedly lower K_D value and a reduced dissociation rate compared to Crocin I, suggesting that Crocin II possesses a superior binding capability. These findings confirm that Crocin II stably binds to ANGPTL8 and exhibits stronger binding capacity than Crocin I. Hence, Crocin II was identified as the optimal candidate for ANGPTL8-targeted intervention.

To characterize the conformational flexibility of the protein structures and the stability of Crocin II-ANGPTL8 (Human) complexes, all-atom MD simulations of 200 ns were performed using GROMACS Post-simulation, the software's built-in tools were utilized to analyze trajectories and compute key metrics: root mean square deviation (RMSD), root mean square fluctuation (RMSF), hydrogen bond occupancy, radius of gyration (Rg), and free-energy landscapes. As shown in Fig. 1i, although the conformation of the ANGPTL8 protein underwent changes during the simulation (with the amino acid residues in its N-terminal region gradually folding and compacting towards the middle), the Crocin II molecule remained stably bound to the ANGPTL8 protein throughout the process. Notably, the RMSD profiles after 140 ns exhibited minimal fluctuations, confirming stable structural dynamics of human ANGPTL8 (Fig. 1j). RMSF analysis revealed residue-specific flexible motions and conformational changes (Fig. 1k). The radius of gyration remained stable throughout the simulation, reflecting consistent structural integrity and robust intermolecular interactions (Fig. 1l). Meanwhile, backbone hydrogen bond analysis revealed that persistent hydrogen bonding existed in the Crocin II-ANGPTL8 complex (Fig. 1m). To directly assess complex stability, principal component analysis (PCA) was used to extract the first two principal components from RMSD and radius of gyration values. These components were integrated with Gibbs free energy as the *Z*-axis to generate 2D/3D free-energy landscapes, which revealed a well-defined energy minimum cluster (Fig. 1n and o). These results confirmed that the Crocin II-ANGPTL8 complex maintained structural stability.

Crocin II promotes the degradation of ANGPTL8 protein through the autophagosome-lysosome pathway

CCK-8 assays demonstrated that Crocin II exhibited no significant toxicity in mouse PHs across the tested concentration range (Supplementary Fig. S2a), indicating 10–100 μmol·L^{-1} as a safe dosage window for subsequent experiments. Western blot analysis revealed that Crocin II remarkably reduced intracellular protein abundance and secreted levels of ANGPTL8 in mouse PHs in a dose- and time-dependent manner (Fig. 2a–d, Supplementary Fig. S2b and S2c). Notably, a cycloheximide (CHX) chase experiment showed that Crocin II accelerated ANGPTL8 protein degradation, reducing its half-life to 6.45 h (Fig. 2e). We next inhibited proteolytic pathways using MG132 (a proteasome inhibitor) and Bafilomycin A1 (Baf A1, an autophagosome-lysosome fusion inhibitor) to dissect the degradation mechanism. As shown in Fig. 2f, Baf A1 treatment partially abrogated Crocin II-mediated ANGPTL8 degradation, implicating the autophagosome-lysosome pathway in this process (Supplementary Fig. S2d). Consistently, Crocin II bona fide induced autophagic activation as reflected by increased LC3B-II expression and decreased P62 levels (Fig. 2g; Supplementary Fig. S2e). Since ANGPTL8 can directly bind to P62 to form a complex[17], we then validated the binding capacity between Crocin II and human P62 using MOE-based molecular docking assay. The results showed a binding score of −7.76 (Supplementary Fig. S2f), indicating a favorable binding interaction between Crocin II and P62, which facilitates the efficient sequestration of ANGPTL8 into autophagosomes. TEM analysis revealed that while control cells displayed double-membrane autophagosomes, Crocin II induced accumulation of phagophore structures (Fig. 2h). In addition, a marked increase in mCherry-eGFP double-labeled autolysosome was observed in mouse PHs treated with Crocin II (Fig. 2i). A follow-up CHX chase experiment confirmed that Baf A1 completely abolished Crocin II-induced ANGPTL8 degradation, extending its half-life to 19.95 h (Fig. 2j). This data demonstrates that Crocin II promotes ANGPTL8 degradation *via* the autophagosome-lysosome pathway.

ANGPTL8 mediates the lipid-lowering effects of Crocin II in mouse PHs

Given the regulatory role of ANGPTL8 in lipid metabolism, we investigated its direct impact and the efficacy of Crocin II on lipid homeostasis in mouse PHs. ORO and Nile Red staining revealed that 40 nmol·L^{-1} recombinant ANGPT8 protein increased the lipid contents, whereas Crocin II pretreatment dose-dependently led to a significant retardation of this accumulation in mouse PHs (Supplementary Fig. S3a and S3b). These results were confirmed by cellular TG concentration tests (Supplementary Fig. S3c). Subsequently, RT-qPCR analyses were performed on key lipid metabolic genes. As shown in Fig. 3b, *Angptl8* significantly upregulated the mRNA expression of lipogenic genes critical for *de novo* monounsaturated fatty acid synthesis (*Fasn*, *Dgat1*, *Cidea*), whereas Crocin II reversed this induction (Supplementary Fig. S3d). Concurrently, *Angptl8* suppressed the mRNA levels of lipolytic genes (*Atgl*, *Hsl*), while Crocin II markedly antagonized these inhibitory effects (Supplementary Fig. S3e). Additionally, hepatic mRNA levels of FAO-related genes (*Pparα*, *Acox1*, *Cpt1a*) were minimally affected by either treatment (Supplementary Fig. S3f). Furthermore, Western blot analysis confirmed that Crocin II counteracted ANGPTL8's detrimental effects on lipogenic and lipolytic protein expression (Supplementary Fig. S3g and S3h). This data demonstrates that ANGPTL8 promotes lipid accumulation in mouse PHs by enhancing lipogenesis and inhibiting lipolysis, whereas Crocin II exerts opposing effects.

To validate Crocin II's therapeutic potential against hepatic steatosis, we employed an *in vitro* model of FFA-induced lipid overload. As visualized by ORO and Nile Red staining, pretreatment with Crocin II dose-dependently attenuated FFA-induced excessive lipid accumulation in mouse PHs (Fig. 3a; Supplementary Fig. S4a). This lipid-lowering effect of Crocin II was confirmed by reduced intracellular TG levels (Supplementary Fig. S4b). At the molecular level, Crocin II counteracted FFA-driven upregulation of lipogenic genes (*Fasn*, *Dgat1*, *Cidea*) and restored expression of the lipolytic gene *Atgl* at both mRNA and protein levels (Fig. 3b). Notably, FFA treatment significantly increased ANGPTL8 protein expression, whereas Crocin II decreased its protein levels in a concentration-dependent manner (Fig. 3c; Supplementary Fig. S4c). These findings establish that Crocin II could target ANGPTL8 and mitigate FFA-induced steatosis in mouse PHs.

Given the lipid-regulatory role of *Angptl8*, we next examined the potential relationship between *Angptl8* deficiency in mouse PHs and the reduction of FFA-induced lipid accumulation by Crocin II. Our results showed that, whereas both Crocin II treatment and *Angptl8* deficiency decreased lipid accumulation in mouse PHs, Crocin II failed to elicit a further reduction of lipid contents in FFA-treated mouse PHs (Fig. 3d; Supplementary Fig. S4d and S4e). At the molecular level, the FFA-orchestrated hepatic expression of *Fasn*,

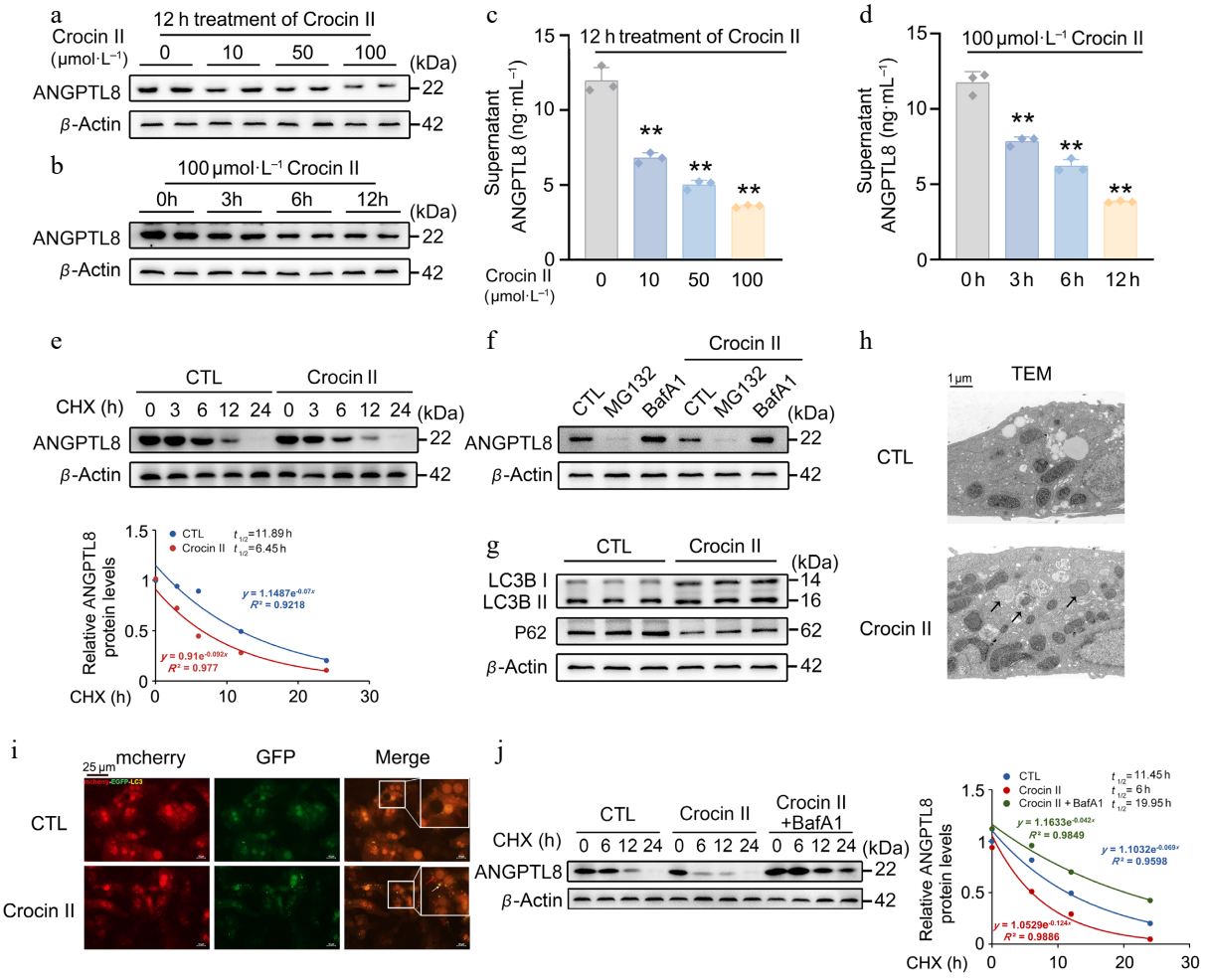

Fig. 2 Crocin II promotes the degradation of ANGPTL8 protein through the autophagosome-lysosome pathway. (a) The protein levels of ANGPTL8 in mouse PHs treated with different concentrations of Crocin II for 12 h. (b) The protein levels of ANGPTL8 in mouse PHs treated with 100 μmol·L^{-1} Crocin II for different time points. (c) Supernatant ANGPTL8 levels in mouse PHs treated with indicated different concentrations of Crocin II for 12 h. (d) Supernatant ANGPTL8 levels in mouse PHs treated with 100 μmol·L^{-1} Crocin II for different durations. (e) CHX chase assay to assess Crocin II-induced changes in ANGPTL8 protein stability in mouse PHs. CTL, control. (f) Western blot analysis of ANGPTL8 protein degradation pathways. (g) The protein levels of LC3B-II/I and P62 in mouse PHs treated with 100 μmol·L^{-1} Crocin II. (h) TEM analysis (arrows indicate autophagosomes). (i) mCherry-eGFP-LC3 fluorescence images (white arrows indicate autophagosomes, and the red arrows indicate autolysosomes), scale bar = 25 μm. (j) The protein levels of ANGPTL8 in mouse PHs treated with Crocin II or combined with BafA1. ** $P < 0.01$ vs 0 μmol·L^{-1} Crocin II group, one-way ANOVA followed by Bonferroni's post hoc test. Data are presented as the mean ± SEM, $n = 3$.

Dgat1 and *Cidea* was normalized by Crocin II and *Angptl8* deficiency (Fig. 3e and f; Supplementary Fig. S4f). In parallel, we overexpressed *Angptl8* in mouse PHs to validate the mediating role of *Angptl8* in Crocin II's lipid-lowering properties. The overexpression efficacy of *Angptl8* was presented in Fig. 3g and Supplementary Fig. S4g. As shown in Fig. 3h, *Angptl8* overexpression partially abrogated the inhibitory effect of Crocin II on FFA-induced lipid accumulation (Supplementary Fig. S4h and S4i). Meanwhile, such an overexpression significantly retarded the Crocin II-induced normalization of lipid metabolic gene expression in FFA-treated PHs (Fig. 3i; Supplementary Fig. S4j). These findings suggest that ANGPTL8 serves as a bona fide target of Crocin II, which mediates its lipid-lowering effects.

Crocin II improves HFD-induced insulin resistance and hyperlipidemia in mice

To further confirm the beneficial effects of Crocin II on hepatic steatosis *in vivo*, mice were fed with an HFD and treated with different doses of Crocin II for 10 weeks (Fig. 4a). HFD feeding significantly reduced food intake in mice, whereas Crocin II administration did not alter either food intake or water drinking across all experimental mice (Supplementary Fig. S5a). Notably, high-dose administration of Crocin II markedly reduced the body weight of HFD-fed mice by 18.58% (Fig. 4b). Morphologically, Crocin II-treated mice exhibited alleviated HFD-induced hepatic steatosis and reduced epididymal fat accumulation (Fig. 4c). GTT and ITT demonstrated that Crocin II dose-dependently improved glucose intolerance and insulin resistance in HFD-fed mice (Fig. 4d; Supplementary Fig. S5b). Biochemically, Crocin II normalized serum lipid profiles by reducing the levels of TG, TC, and LDL-C in HFD-fed mice (Fig. 4e and f). Consistently, the detrimental LDL-C/HDL-C ratio was significantly lowered by Crocin II treatment (Fig. 4f).

Crocin II ameliorates HFD-induced hepatic steatosis in mice

Crocin II administration significantly mitigated HFD-induced fatty liver in mice (Fig. 5a). Quantitatively, HFD feeding induced 0.5-fold and 4.9-fold increases in liver and epididymal fat weights,

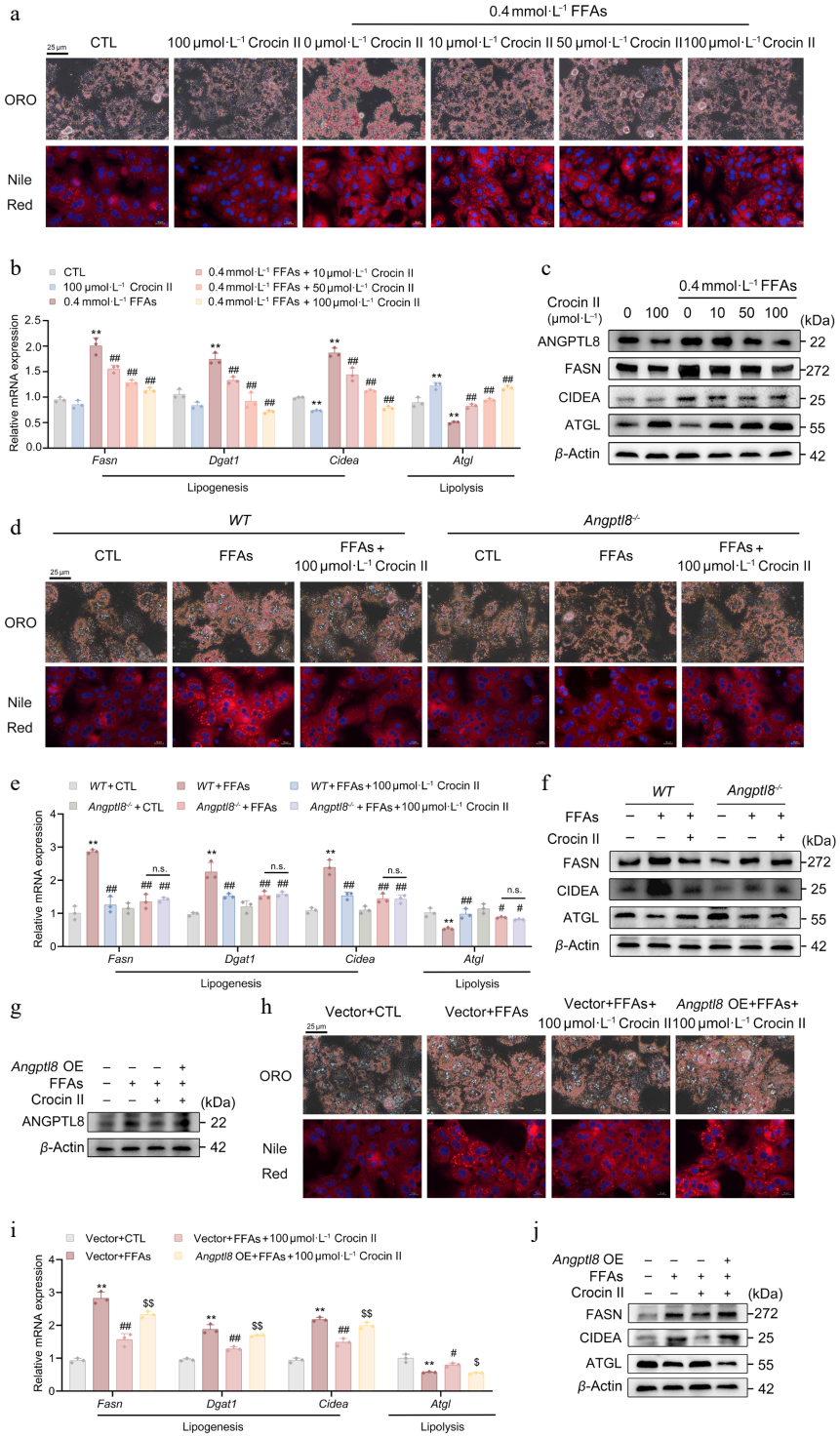

Fig. 3 ANGPTL8 mediates the lipid-lowering effects of Crocin II in mouse PHs. (a)–(c) Mouse PHs were pre-incubated with 100 μmol·L^{-1} Crocin II for 2 h, and then treated with 100 μmol·L^{-1} Crocin II and 0.4 mmol·L^{-1} FFAs for 24 h. (a) ORO staining and Nile Red staining. Scale bar = 25 μm. (b) The relative mRNA expression of *Fasn*, *Dgat1*, *Cidea* and *Atgl*. (c) The protein levels of ANGPTL8, FASN, CIDEA and ATGL. ** $P < 0.01$ vs CTL group, $^{\#} P < 0.05$, $^{\#\#} P < 0.01$ vs 0.4 mmol·L^{-1} FFAs group, one-way ANOVA followed by Bonferroni's post hoc test. (d)–(f) Mouse PHs isolated from WT and *Angptl8*$^{-/-}$ mice were pre-incubated with 100 μmol·L^{-1} Crocin II for 2 h, and then treated with 100 μmol·L^{-1} Crocin II and 0.4 mM FFAs for 24 h. (d) ORO staining and Nile Red staining. Scale bar = 25 μm. (e) The relative mRNA expression of *Fasn*, *Dgat1*, *Cidea* and *Atgl*. (f) The protein levels of FASN, CIDEA and ATGL. n.s., no significance, ** $P < 0.01$ vs WT + CTL group, $^{\#} P < 0.05$ and $^{\#\#} P < 0.01$ vs WT + FFAs group, one-way ANOVA followed by Bonferroni's post hoc test. (g)–(j) Mouse PHs were transfected with either *Angptl8*-overexpressing plasmid or empty vector (pcDNA3.0). 24 h later, cells were pre-incubated with 100 μmol·L^{-1} Crocin II for 2 h, and then treated with 100 μmol·L^{-1} Crocin II and 0.4 mmol·L^{-1} FFAs for 24 h. (g) The protein levels of ANGPTL8. (h) ORO staining and Nile Red staining. Scale bar = 25 μm. (i) The relative mRNA expression of *Fasn*, *Dgat1*, *Cidea* and *Atgl*. (j) The protein levels of FASN, CIDEA and ATGL. *A8oe*, *Angptl8* overexpression. * $P < 0.05$ and ** $P < 0.01$ vs vector + CTL group, $^{\#} P < 0.05$ and $^{\#\#} P < 0.01$ vs vector + FFAs group, or + FFAs group, $^{\$} P < 0.05$, and $^{\$\$} P < 0.01$ vs vector + FFAs + 100 μmol·L^{-1} Crocin II group, one-way ANOVA followed by Bonferroni's post hoc test. Data are presented as the mean ± SEM, $n = 3$.

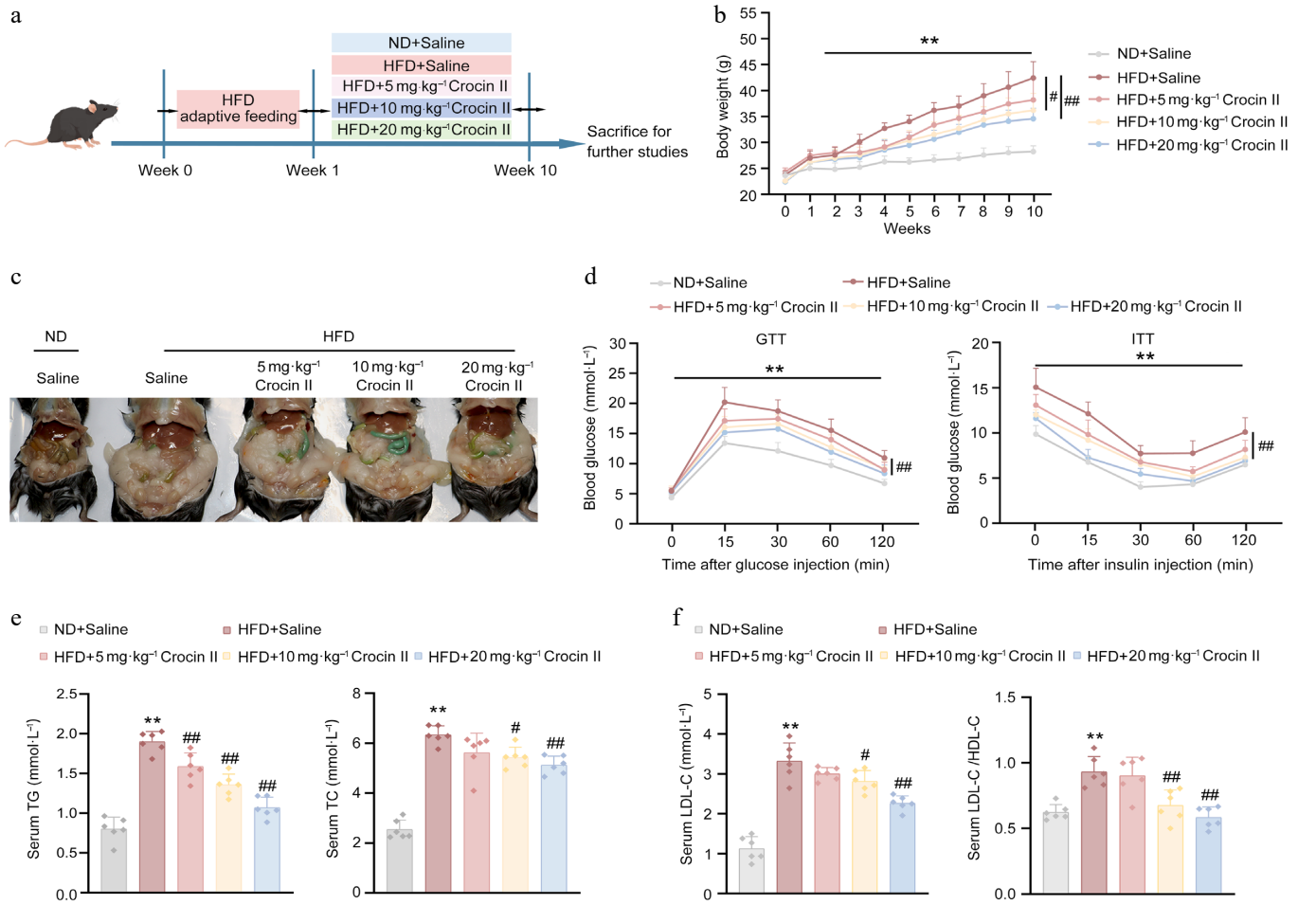

Fig. 4 Crocin II improves HFD-induced insulin resistance and hyperlipidemia in mice. Mice were fed a ND or HFD for 10 weeks to induce MASLD, with or without *i.p.* administration of Crocin II (5, 10, and 20 mg·kg^{-1} body weight) during the 10 weeks. (a) Schematic representation of the experimental animal procedure. (b) Body weight. (c) Morphological photos. (d) GTT and ITT analyses. (e) Serum TG and TC levels. (f) Serum LDL-C levels and the LDL-C/HDL-C ratio. ** $P < 0.01$ vs ND + saline group, $^{\#}P < 0.05$ and $^{\#\#}P < 0.01$ vs HFD + saline group, one-way ANOVA followed by Bonferroni's post hoc test. Data are presented as the mean ± SEM, $n = 6$.

respectively, which were dose-dependently reduced by Crocin II treatment (Fig. 5b). Moreover, serum biomarkers of hepatic injury, ALT and AST, were increased in response to HFD feeding, whereas Crocin II significantly blunted these increases, confirming its hepatoprotective activity (Fig. 5c). Histopathological analysis revealed massive lipid droplet accumulation in H&E-stained liver and epididymal fat sections from HFD-fed mice. Such pathological changes were potently reversed by Crocin II in a dose-dependent manner (Fig. 5d). ORO staining further validated reduced hepatic lipid deposition in Crocin II-treated groups (Fig. 5e; Supplementary Fig. S6a). Biochemically, HFD-induced hepatic TG and TC levels were significantly lowered by Crocin II, with the high dose achieving 48% reduction in TG and 52% reduction in TC (Fig. 5f). Notably, Crocin II also attenuated HFD-induced hepatic macrophage infiltration, as evidenced by reduced F4/80-positive cells (Fig. 5g; Supplementary Fig. S6b). These findings demonstrate that Crocin II effectively ameliorates HFD-induced hepatic lipid accumulation, inflammation, and functional injury, positioning it as a promising candidate for therapeutic development against MASLD.

Crocin II reprograms hepatic lipidomic landscape in HFD-induced MASLD mice

To delineate Crocin II's effects on hepatic lipid metabolism, we performed untargeted lipidomic profiling on livers from HFD-fed MASLD mice administered with or without Crocin II. PCA revealed distinct clustering of lipid signatures among treatment groups (Fig. 6a). Volcano analysis identified 134 lipid species altered by Crocin II (Fig. 6b). These lipids are primarily categorized into glycerolipids (TGs and DGs), glycerophospholipids (PC, PE, and CL), and sterol lipids (ChE) (Fig. 6c). Consistent with histological findings, lipidome analysis showed that glycerolipids (33 TG and 25 DG metabolites), sterol lipids (5 ChE metabolites), and fatty acyls (3 WE metabolites) were significantly reduced in Crocin II-treated livers compared to HFD-fed controls (Fig. 6d). Additionally, the hepatic levels of PC (26 : 1 COOH), PC (38 : 5), PC (18 : 2/18 : 3 COOH), PC (16 : 2 COOH/18 : 2), and PC (16 : 0/16 : 2 COOH) were significantly increased, whereas the levels of PC (21 : 3/18 : 0), PC (39 : 3), PC (27 : 1/11 : 0 CHO), and PC (15 : 1 CHO/16 : 0) were decreased by Crocin II treatment. Moreover, PE (18 : 4/20 : 4), PE (22:6/16:0), PE (6 : 1 CHO/20 : 3), and CL levels were reduced by Crocin II treatment (Supplementary Fig. S7a). However, the total amount of PC exhibited an upregulated trend in response to Crocin II, while the ratio of PC to PE was significantly increased (Supplementary Fig. S7b and S7c). Given that PCs are precursors of VLDL[34], VLDL synthesis may partially underlie the lipid-lowering effects of Crocin II in the liver of HFD-fed mice. At the molecular level, Crocin II reversed HFD-induced dysregulation of lipid metabolism-associated genes. Among which, lipogenic markers *Fasn* and *Dgat1a* were significantly downregulated, while the lipolytic gene *Atgl* was markedly

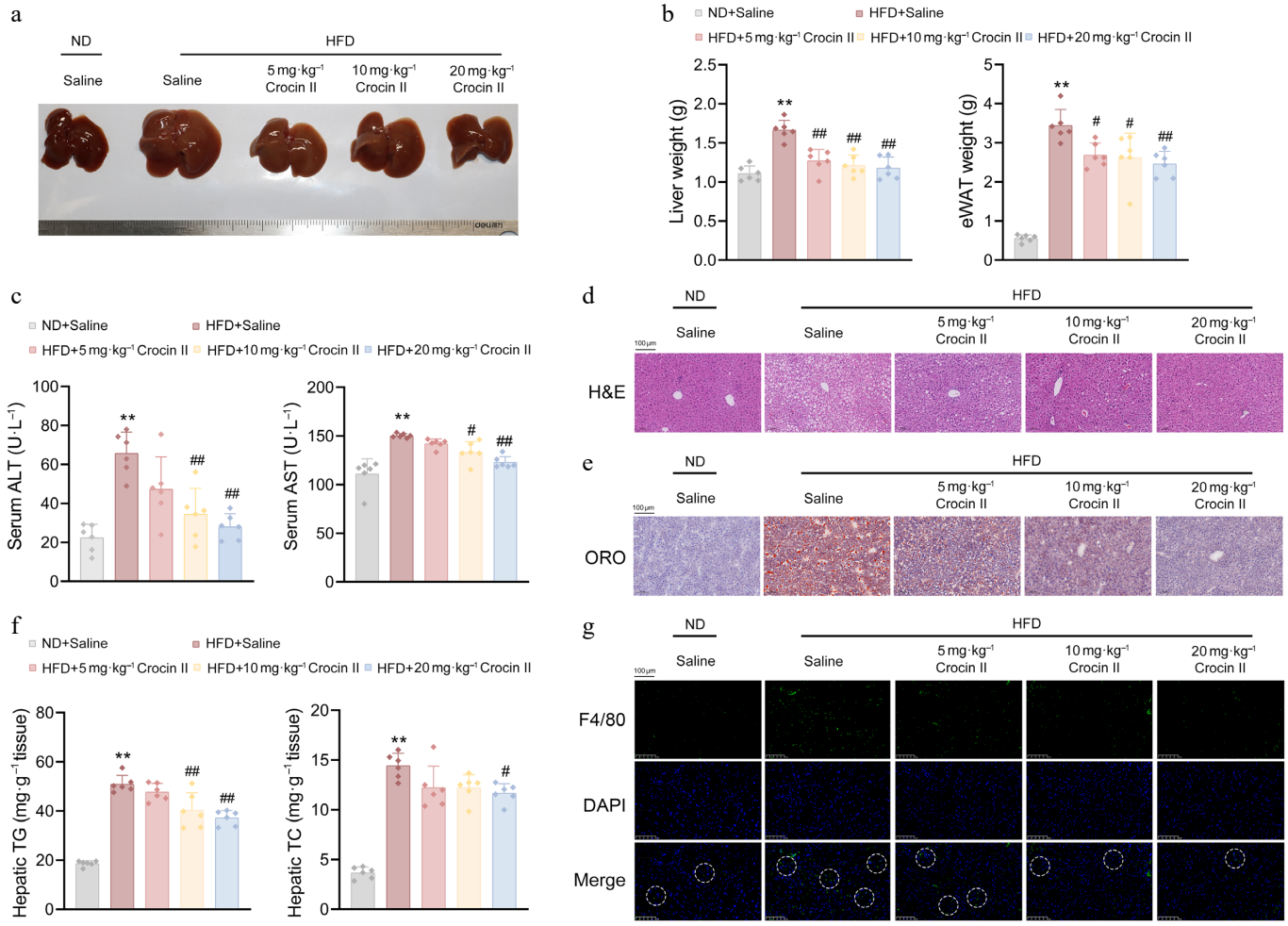

Fig. 5 Crocin II ameliorates HFD-induced hepatic steatosis in mice. (a) Image of liver morphology. (b) Liver and eWAT weights. (c) Serum ALT and AST levels. (d) Representative images of livers by H&E staining. Scale bar = 100 μm. (e) Representative images of livers by Oil Red O staining. Scale bar = 100 μm. (f) Liver TG and TC contents. (g) Representative images showed F4/80 staining of liver tissues. Scale bar = 100 μm. ** $P < 0.01$ vs ND + Saline group, # $P < 0.05$ and ## $P < 0.01$ vs HFD + Saline group, one-way ANOVA followed by Bonferroni's post hoc test. Data are presented as the mean ± SEM, $n = 6$.

upregulated (Fig. 6e). Concomitantly, serum *Angptl8* levels were correspondingly reduced in Crocin II-treated MASLD mice (Fig. 6e). Accordingly, Crocin II dose-dependently decreased HFD-induced ANGPTL8 protein levels in mouse livers (Fig. 6f; Supplementary Fig. S7d). These findings indicate that Crocin II exerts its beneficial effects by targeting ANGPTL8, thereby mitigating HFD-induced hepatic lipid accumulation.

Crocin II exerts *in vivo* organ safety

To assess the potential toxic effects of Crocin II on systemic organs, we measured renal injury biomarkers (creatinine, BUN) and cardiac stress markers (ANP, BNP) in serum samples. As shown in Fig. 7a and b, Crocin II treatment significantly normalized these biochemical biomarkers in the HFD-fed group, indicating its protective effects without inducing overt toxicity. Histological analyses further revealed that Crocin II-treated mice preserved normal tissue architecture and reduced inflammatory cell infiltration in the kidneys, hearts, and spleens, compared to the disrupted morphology and prominent inflammation in HFD-fed controls (Fig. 7c–e). Overall, these results suggest that Crocin II exhibits no detectable organ toxicity *in vivo* and may protect against HFD-induced tissue damage.

Discussion

ANGPTL8 is a secreted glycoprotein that has been documented as a potential therapeutic target for MASLD[35]. Preclinically, neutralization of ANGPTL8 with the monoclonal antibody REGN3776 (Regeneron Pharmaceuticals) accelerates TG clearance and normalizes plasma TG levels in dyslipidemic murine and cynomolgus monkeys[23]. However, the substantial costs associated with manufacturing and administering this neutralizing antibody may limit its clinical application. Additionally, considering the physiological function of ANGPTL8, non-selective regulation of ANGPTL8 by monoclonal antibodies may cause undesirable side effects, such as circadian disruption[15]. Hence, identifying a safe and controllable drug which could precisely degrade excessive ANGPTL8 proteins under pathological settings is of great importance. Herein, we screened Crocin II from natural saffron and identified it as a potential ANGPTL8-targeting agent that facilitates protein degradation of hepatic ANGPTL8 through the autophagosome-lysosome pathway. Pharmacodynamically, Crocin II inhibits lipogenesis and partially restores lipolytic ability in both FFA-treated mouse PHs and the steatotic liver of HFD-induced MASLD mice. Collectively, our findings identify that Crocin II functions as a natural inducer for

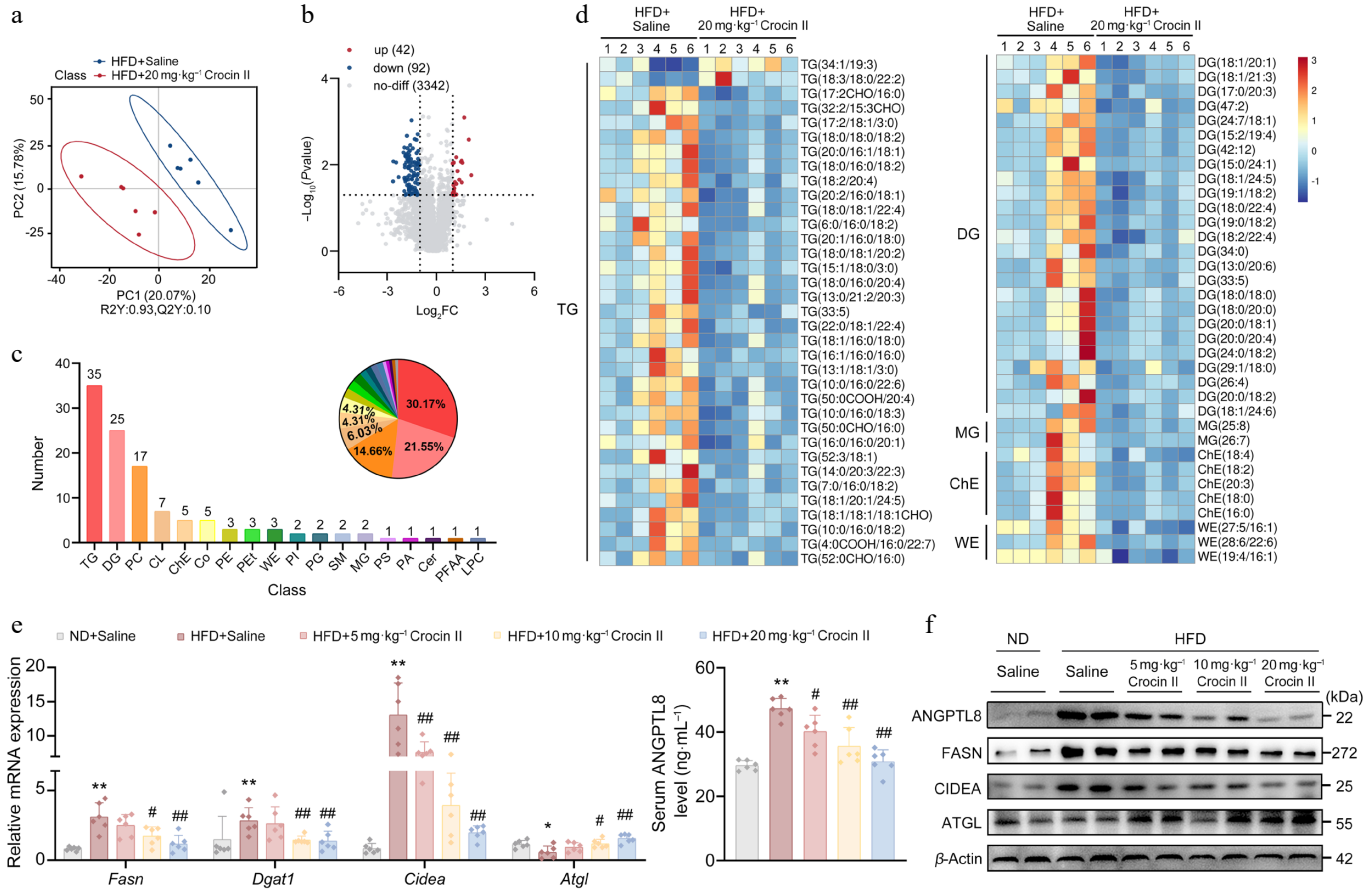

Fig. 6 Crocin II reprograms hepatic lipidomic landscape in HFD-induced MASLD mice. (a) PLS-DA score of liver lipidome in mice from HFD + saline group and HFD + 20 mg·kg^{-1} Crocin II group. (b) Volcano plot. (c) Statistical plot of differential lipid categories. (d) Heatmap of differential lipids. (e) The relative mRNA expression of *Fasn*, *Dgat1*, and *Cidea* (left). The supernatant *Angptl8* levels in mouse serum detected (right). (f) The protein levels of ANGPTL8, FASN, DGAT1 and CIDEA. ** $P < 0.01$ vs ND + saline group, $^{\#}P < 0.05$ and $^{\#\#}P < 0.01$ vs HFD + saline group, one-way ANOVA followed by Bonferroni's post hoc test. Data are presented as the mean ± SEM, $n = 6$.

ANGPTL8 degradation, reinforcing ANGPTL8's value as a therapeutic target for metabolic diseases.

Because of its nutritional and medicinal properties, saffron is well-recognized as a functional food[36], exhibiting health-promoting benefits, including antidepressant effects and potential therapeutic properties in metabolic syndromes[37]. Hence, saffron was selected as a natural source for screening ANGPTL8-targeting natural monomers with specific binding affinity. In our study, as the primary bioactive components of saffron, Crocin I and Crocin II exhibited high binding potentials to ANGPTL8 protein *in silico*. CETSA, DARTS, and SPR analyses revealed that Crocin II directly bound to ANGPTL8 and triggered its protein degradation. Interestingly, CETSA and DARTS assays did not reveal an obvious increase in protein stability of ANGPTL8 with the treatment of Crocin II. In fact, Crocin II even reduced ANGPTL8 protein levels in both assays. These findings seem to be contradictory to our main conclusion. However, specific ligand-protein interactions do not always enhance the stability of target proteins. This type of binding process can induce conformational changes in the target protein that include exposing protease cleavage sites or disrupting intramolecular stabilizing interactions. Such conformational changes may also reduce thermal stability and increase protease susceptibility. For example, both CETSA and DARTS analyses revealed that Hyperibone J could bind to adenosine kinase (ADK), reducing its thermal stability and promoting protease-mediated cleavage[38]. Hence, our CETSA and DARTS assays sufficiently confirm the direct binding of Crocin II to ANGPTL8, and also reflect the changes in ANGPTL8 protein stability to a certain extent. Additionally, GROMACS-based MD simulations further characterized the conformational flexibility of protein structures and the stability of Crocin II-ANGPTL8 complexes. The stronger binding of Crocin II to ANGPTL8 relative to Crocin I is likely related to differences in hydrogen bond formation at the binding interface[39]. Briefly, Crocin II formed six hydrogen bonds with human ANGPTL8, which may contribute to altering ANGPTL8 protein stability. Structurally, Crocin II differs from Crocin I by possessing a monosaccharide rather than a disaccharide glycosidic chain, resulting in higher lipophilicity. This property may enhance membrane permeability and increase contact probability, thereby promoting ANGPTL8 degradation.

As is known, P62, a classic selective autophagy receptor, acts as a key hub linking target proteins to the autophagic machinery[40]. Additionally, ANGPTL8 can directly bind to P62 to form a complex, thereby promoting the selective autophagic degradation of IKKγ[17]. This finding validates the endogenous interaction between ANGPTL8 and P62, and this P62-dependent interaction provides an important molecular basis for autophagic regulation. In our study, we found a favorable binding interaction between Crocin II and P62, thus hypothesizing that Crocin II can bind to ANGPTL8 and P62 individually and may function similarly to proteolysis-targeting chimeras (PROTAC). This dual binding enhances the ANGPTL8-P62 interaction and promotes the formation of the ANGPTL8-P62 complex, which further binds to LC3 on the autophagosomal membrane *via* the LIR motif of P62, consequently facilitating the

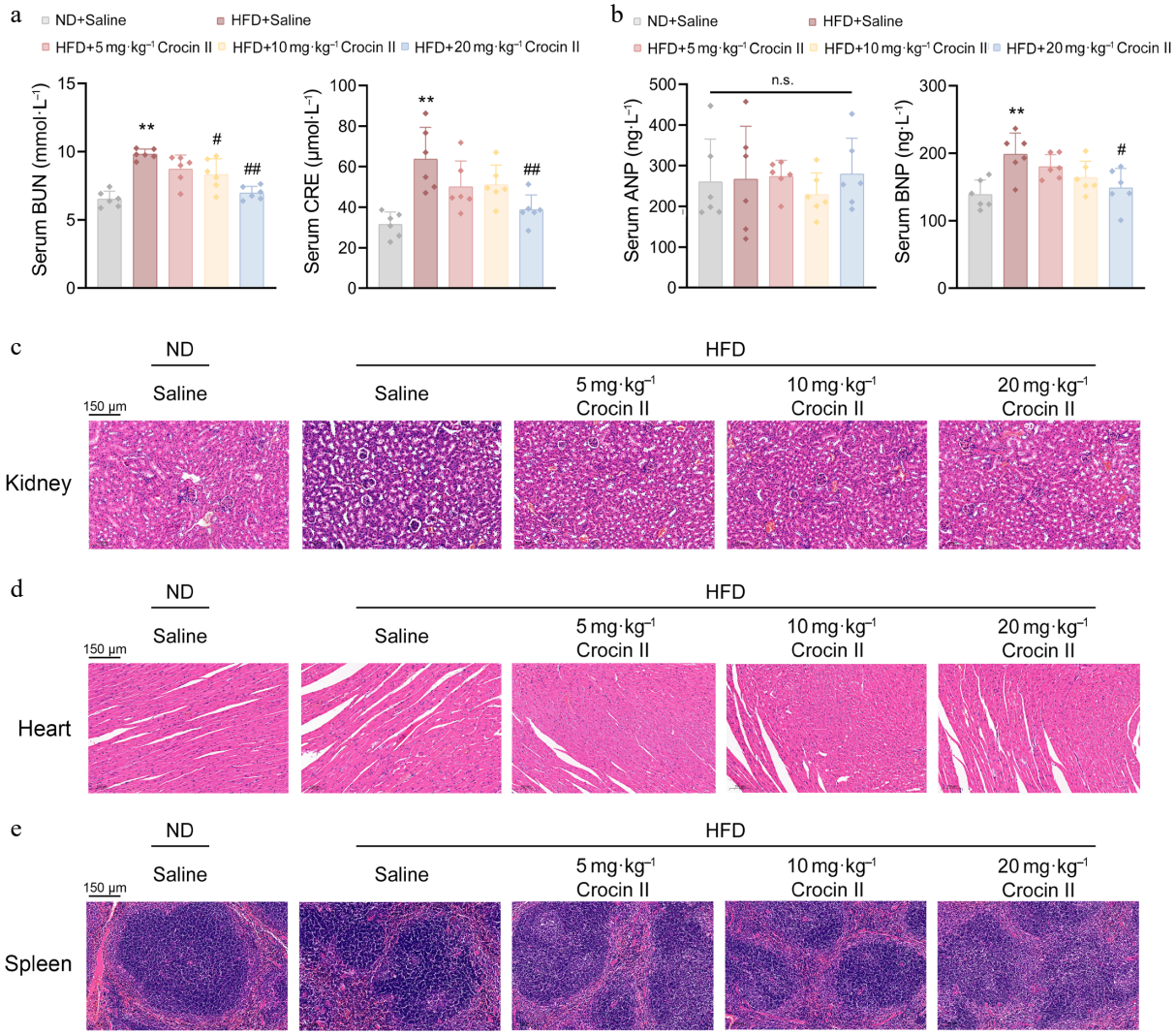

Fig. 7 Crocin II exerts *in vivo* organ safety. (a) The serum levels of BUN and CRE. (b) The serum levels of ANP and BNP. (c) Representative images of the kidney by H&E staining. (d) Representative images of the heart by H&E staining analysis. (d) Representative images of the spleen by H&E staining analysis. n.s., no significance, ** $P < 0.01$ vs ND + saline group, $^{\#}P < 0.05$ and $^{\#\#}P < 0.01$ vs HFD + saline group, one-way ANOVA followed by Bonferroni's post hoc test.Data are presented as the mean ± SEM, $n = 6$.

efficient sequestration of ANGPTL8 into autophagosomes and ultimately promoting ANGPTL8 degradation through the autophagosome-lysosome pathway. Compared with the existing ANGPTL8-targeting strategies that rely on ASOs or monoclonal antibodies, this Crocin II-triggered ANGPTL8 degradation provides a new strategy for discovering druggable PROTAC-like molecules from natural compounds, while offering a cost-effective and low-toxicity alternative to synthetic drugs.

Crocin is a primary bioactive component of saffron. Its beneficial effects include anti-inflammatory, anticancer, cardioprotective, and neuroprotective properties[41,42]. Of note, Crocin has been demonstrated to rectify the imbalance of inflammatory states in patients with metabolic syndromes[43]. Moreover, its major active ingredient, Crocin I effectively enhances insulin sensitivity and reshapes lipid profiles in mice with chronic corticosterone treatment[44]. However, few studies have explored the efficacy of Crocin II on MASLD therapy. Herein, we elucidated the beneficial effects of Crocin II on hepatic lipid profiles under MASLD conditions. In particular, Crocin II reduced hepatic levels of glycerolipids (TGs, DGs, and MGs) and sterol lipids (ChE) in HFD-induced MASLD mice. Consistently, Crocin II attenuated ANGPTL8- and FFA-induced upregulation of DG/TG synthesis-related genes (*Fasn*, *Dgat1*, *Cidea*) at the mRNA level. Importantly, PC and PE constitute the major phospholipid components, which maintain the integrity of the lipid droplet surface[45]. A reduction of the PC/PE ratio compromises this barrier function, thus promoting excessive accumulation of TG and cholesterol in lipid droplets on the droplet surface. Such an aggregation contributes to the progression from hepatic steatosis to MASH in MASLD[46,47]. Additionally, a reduction of PC content leads to abnormal protein folding of apolipoprotein B100, thereby impairing the assembly and secretion efficiency of VLDL[34,46]. In our study, we found that Crocin II treatment increased total hepatic PC levels and elevated the PC/PE ratio in mice. Meanwhile, the corresponding elevations were accompanied by reduced intrahepatic lipid accumulation. These findings suggest the beneficial effects of Crocin II on lipid deposition on the droplet surface, while ANGPTL8 may be involved in this process.

On the other hand, given the key regulatory function of ANGPTL8 in hepatic TG homeostasis, whether Crocin II regulates TG and DG lipids in an ANGPTL8-dependent manner warrants further investigation. To address this, loss- and gain-of-function approaches were applied to manipulate the ANGPTL8 expression in mouse PHs, confirming that ANGPTL8 served as a *bona fide* target of Crocin II.

Notably, an *Angptl8*-deficient mouse model would be valuable for assessing the Crocin II–ANGPTL8 interaction and its benefits on MASLD. However, *Angptl8* deficiency intrinsically protects mice from diet-induced hepatic steatosis[21], precluding the demonstration that Crocin II's beneficial effects on MASLD are abolished in *Angptl8*-deficient mice. Future studies employing liver-specific gene modulation using an AAV8-TBG delivery system may help to overcome this limitation. Additionally, ANGPTL8 acts as a circadian *Zeitgeber* in regulating lipid clocks in the liver[15], thus, the optimal administration window for Crocin II and whether it restores lipid clocks by targeting ANGPTL8 in MASLD mice represent intriguing avenues for future research.

Pharmacological agents, such as pioglitazone, obeticholic acid, and the THRβ agonist resmetirom, have been evaluated for MASLD treatment. However, their clinical use is constrained by adverse effects and metabolic complications[48,49]. For example, obeticholic acid may induce pruritus, gastrointestinal discomfort, and liver dysfunction[50]. Hence, these challenges highlight the importance of identifying alternative therapeutic drugs with better tolerability profiles. In our study, Crocin II significantly antagonized HFD-induced liver injury, as evidenced by reduced serum AST and ALT levels and decreased F4/80-positive macrophage infiltration. No obvious pathological alterations were detected in the kidneys or hearts following Crocin II treatment. Interestingly, a clinical trial showed that 15 mg/d Crocin tablets for 90 d in healthy individuals caused only modest changes in blood parameters, without any other adverse effects[47]. Therefore, as a food-derived agent, Crocin II may represent a promising candidate for MASLD treatment.

In summary, given the prominent druggable potential of ANGPTL8 in MASLD, we identify Crocin II as a novel natural ANGPTL8-degrading inducer that specifically facilitates hepatic ANGPTL8 degradation *via* the autophagosome-lysosome pathway. Thus, Crocin II serves as a safe, cost-effective, and promising therapeutic candidate for MASLD.

Ethical statements

All animal procedures in this study were conducted in accordance with the Guide for the Care and Use of Laboratory Animals, published by the US National Institutes of Health (NIH publication No. 85-23, revised 1996), and the approved regulations set by the Laboratory Animal Care Committee at China Pharmaceutical University (LACUC Issue No: 2024-05-064, approval date: 2024-05-27).

Author contributions

The authors confirm contributions to the work as follows: study conception and design: Chen S, Zhang W; data collection: Zhang R, Li K, Zhao Z, Jiang X, Zhang R, Liu C; analysis and interpretation of results: Zhang R, Li K; draft manuscript preparation: Zhang R, Li K; manuscript revision and editing: Chen S, Zhang W. All authors reviewed the results and approved the final version of the manuscript.

Data availability

Data supporting this study are included in the article and supplementary files or available from the corresponding author on request.

Acknowledgments

This work was financially supported by grants from the National Key R&D Program of China (Grant No. 2022YFA0807200), the National Natural Science Foundation of China (Grant No. 32471201), the Natural Science Foundation of Jiangsu Province (Grant No. BK20220151), the Project of State Key Laboratory of Natural Medicines, China Pharmaceutical University (no. SKLNMZZ2024JS34), the Open Research Fund of Yunnan Characteristic Plant Extraction Laboratory (Grant No. YKKF2024018), the Priority Academic Program Development of Jiangsu Higher Education Institutions (PAPD), and The National Innovation and Entrepreneurship Training Program for Undergraduates.

Conflict of interest

The authors declare that there is no conflict of interest.

Supplementary information accompanies this paper online at: https://doi.org/10.48130/targetome-0026-0012.

Dates

Received 9 January 2026; Revised 30 January 2026; Accepted 23 February 2026; Published online 3 April 2026

References

[1] Syed-Abdul MM. 2023. Lipid metabolism in metabolic-associated steatotic liver disease (MASLD). *Metabolites* 14:12

[2] Miao L, Targher G, Byrne CD, Cao YY, Zheng MH. 2024. Current status and future trends of the global burden of MASLD. *Trends in Endocrinology & Metabolism* 35:697–707

[3] Chan WK, Chuah KH, Rajaram RB, Lim LL, Ratnasingam J, et al. 2023. Metabolic dysfunction-associated steatotic liver disease (MASLD): a state-of-the-art review. *Journal of Obesity & Metabolic Syndrome* 32:197–213

[4] Sandireddy R, Sakthivel S, Gupta P, Behari J, Tripathi M, et al. 2024. Systemic impacts of metabolic dysfunction-associated steatotic liver disease (MASLD) and metabolic dysfunction-associated steatohepatitis (MASH) on heart, muscle, and kidney related diseases. *Frontiers in Cell and Developmental Biology* 12:1433857

[5] Le MH, Yeo YH, Zou B, Barnet S, Henry L, et al. 2022. Forecasted 2040 global prevalence of nonalcoholic fatty liver disease using hierarchical bayesian approach. *Clinical and Molecular Hepatology* 28:841–850

[6] Younossi ZM, Stepanova M, Ong J, Trimble G, AlQahtani S, et al. 2021. Nonalcoholic steatohepatitis is the most rapidly increasing indication for liver transplantation in the United States. *Clinical Gastroenterology and Hepatology* 19:580–589.e5

[7] Hagström H, Shang Y, Hegmar H, Nasr P. 2024. Natural history and progression of metabolic dysfunction-associated steatotic liver disease. *The Lancet Gastroenterology & Hepatology* 9:944–956

[8] Younossi ZM, Kalligeros M, Henry L. 2025. Epidemiology of metabolic dysfunction-associated steatotic liver disease. *Clinical and Molecular Hepatology* 31:S32–S50

[9] Stefan N, Yki-Järvinen H, Neuschwander-Tetri BA. 2025. Metabolic dysfunction-associated steatotic liver disease: heterogeneous pathomechanisms and effectiveness of metabolism-based treatment. *The Lancet Diabetes & Endocrinology* 13:134–148

[10] Nguyen M, Asgharpour A, Dixon DL, Sanyal AJ, Mehta A. 2024. Emerging therapies for MASLD and their impact on plasma lipids. *American Journal of Preventive Cardiology* 17:100638

[11] Machado MV. 2023. MASLD treatment-a shift in the paradigm is imminent. *Frontiers in Medicine* 10:1316284

[12] Sylvers-Davie KL, Davies BSJ. 2021. Regulation of lipoprotein metabolism by ANGPTL3, ANGPTL4, and ANGPTL8. *American Journal of Physiology Endocrinology and Metabolism* 321:E493–E508

[13] Luo M, Peng D. 2018. ANGPTL8: an important regulator in metabolic disorders. *Frontiers in Endocrinology* 9:169

[14] Guo C, Wang C, Deng X, He J, Yang L, et al. 2021. ANGPTL8 in metabolic homeostasis: more friend than foe? *Open Biology* 11:210106

[15] Chen S, Feng M, Zhang S, Dong Z, Wang Y, et al. 2019. ANGPTL8 mediates food-driven resetting of hepatic circadian clock in mice. *Nature Communications* 10:3518
[16] Petrescu M, Vlaicu SI, Ciumărnean L, Milaciu MV, Mărginean C, et al. 2022. Chronic inflammation-a link between nonalcoholic fatty liver disease (NAFLD) and dysfunctional adipose tissue. *Medicina* 58:641
[17] Zhang Y, Guo X, Yan W, Chen Y, Ke M, et al. 2017. ANGPTL8 negatively regulates NF-κB activation by facilitating selective autophagic degradation of IKKγ. *Nature Communications* 8:2164
[18] Feng Y, Luo S, Fang C, Ma S, Fan D, et al. 2024. ANGPTL8 deficiency attenuates lipopolysaccharide-induced liver injury by improving lipid metabolic dysregulation. *Journal of Lipid Research* 65:100595
[19] Su Y, Zhang R, Li K, Shen H, Nan M, et al. 2025. Angiopoietin-like protein 8 orchestrates macrophage glycogen metabolism and polarization via the JNK signaling pathway in cytokine storm syndrome. *Cell & Bioscience* 15:140
[20] Li DP, Huang L, Kan RR, Meng XY, Wang SY, et al. 2023. LILRB2/PirB mediates macrophage recruitment in fibrogenesis of nonalcoholic steatohepatitis. *Nature Communications* 14:4436
[21] Zhang Z, Yuan Y, Hu L, Tang J, Meng Z, et al. 2023. ANGPTL8 accelerates liver fibrosis mediated by HFD-induced inflammatory activity *via* LILRB2/ERK signaling pathways. *Journal of Advanced Research* 47:41–56
[22] Vatner DF, Goedeke L, Camporez JG, Lyu K, Nasiri AR, et al. 2018. ANGPTL8 antisense oligonucleotide improves adipose lipid metabolism and prevents diet-induced NAFLD and hepatic insulin resistance in rodents. *Diabetologia* 61:1435–1446
[23] Gusarova V, Banfi S, Alexa-Braun CA, Shihanian LM, Mintah IJ, et al. 2017. ANGPTL8 blockade with a monoclonal antibody promotes triglyceride clearance, energy expenditure, and weight loss in mice. *Endocrinology* 158:1252–1259
[24] Goyenvalle A, Jimenez-Mallebrera C, van Roon W, Sewing S, Krieg AM, et al. 2023. Considerations in the preclinical assessment of the safety of antisense oligonucleotides. *Nucleic Acid Therapeutics* 33:1–16
[25] Hansel TT, Kropshofer H, Singer T, Mitchell JA, George AJ. 2010. The safety and side effects of monoclonal antibodies. *Nature Reviews Drug Discovery* 9:325–338
[26] Li J, Lei HT, Cao L, Mi YN, Li S, et al. 2018. Crocin alleviates coronary atherosclerosis via inhibiting lipid synthesis and inducing M2 macrophage polarization. *International Immunopharmacology* 55:120–127
[27] Chen S, Qian J, Shi X, Gao T, Liang T, et al. 2014. Control of hepatic gluconeogenesis by the promyelocytic leukemia zinc finger protein. *Molecular Endocrinology* 28:1987–1998
[28] Chen S, Li X, Liu L, Liu C, Han X. 2018. Ophiopogonin D alleviates high-fat diet-induced metabolic syndrome and changes the structure of gut microbiota in mice. *FASEB Journal* 32:1139–1153
[29] Lu T, Chen F. 2012. Multiwfn: a multifunctional wavefunction analyzer. *Journal of Computational Chemistry* 33:580–592
[30] Lu T. 2024. A comprehensive electron wavefunction analysis toolbox for chemists, Multiwfn. *The Journal of Chemical Physics* 161:082503
[31] Kimura S, Noda T, Yoshimori T. 2007. Dissection of the autophagosome maturation process by a novel reporter protein, tandem fluorescent-tagged LC3. *Autophagy* 3:452–460
[32] Shui G, Cheong WF, Jappar IA, Hoi A, Xue Y, et al. 2011. Derivatization-independent cholesterol analysis in crude lipid extracts by liquid chromatography/mass spectrometry: applications to a rabbit model for atherosclerosis. *Journal of Chromatograph A* 1218:4357–4365
[33] Ru J, Li P, Wang J, Zhou W, Li B, et al. 2014. TCMSP: a database of systems pharmacology for drug discovery from herbal medicines. *Journal of Cheminformatics* 6:13
[34] Sherriff JL, O'Sullivan TA, Properzi C, Oddo JL, Adams LA. 2016. Choline, its potential role in nonalcoholic fatty liver disease, and the case for human and bacterial genes. *Advances in Nutrition* 7:5–13
[35] Gaudet D, Gonciarz M, Shen X, Leohr JK, Beyer TP, et al. 2025. Targeting the angiopoietin-like protein 3/8 complex with a monoclonal antibody in patients with mixed hyperlipidemia: a phase 1 trial. *Nature Medicine* 31:2632–2639
[36] Tufail T, Ain HBU, Ikram A, Arshad MT, Abdullahi MA. 2025. Functional, nutraceutical and health endorsing perspectives of saffron. *Food Science & Nutrition* 13:e70721
[37] José Bagur M, Alonso Salinas GL, Jiménez-Monreal AM, Chaouqi S, Llorens S, et al. 2017. Saffron: an old medicinal plant and a potential novel functional food. *Molecules* 23:30
[38] Li T, Li Y, Chen J, Nan M, Zhou X, et al. 2025. Hyperibone J exerts antidepressant effects by targeting ADK to inhibit microglial P2X7R/TLR4-mediated neuroinflammation. *Journal of Advanced Research* 72:571–589
[39] Hassan M, Coutsias EA. 2021. Protein secondary structure motifs: a kinematic construction. *Journal of Computational Chemistry* 42:271–292
[40] Lamark T, Svenning S, Johansen T. 2017. Regulation of selective autophagy: the P62/SQSTM1 paradigm. *Essays in Biochemistry* 61:609–624
[41] Bastani S, Vahedian V, Rashidi M, Mir A, Mirzaei S, et al. 2022. An evaluation on potential anti-oxidant and anti-inflammatory effects of Crocin. *Biomedicine & Pharmacotherapy* 153:113297
[42] Pourmousavi L, Asadi RH, Zehsaz F, Jadidi RP. 2024. Potential therapeutic effects of crocin. *Naunyn-Schmiedeberg's Archives of Pharmacology* 397:7395–7420
[43] Nikbakht-Jam I, Khademi MM, Nosrati M, Eslami S, Foroutan-Tanha M, et al. 2016. Effect of crocin extracted from saffron on pro-oxidant–anti-oxidant balance in subjects with metabolic syndrome: a randomized, placebo-controlled clinical trial. *European Journal of Integrative Medicine* 8:307–312
[44] Xie X, Xiao Q, Xiong Z, Yu C, Zhou J, et al. 2019. Crocin-I ameliorates the disruption of lipid metabolism and dysbiosis of the gut microbiota induced by chronic corticosterone in mice. *Food & Function* 10:6779–6791
[45] Chin CF, LA Galam D, Gao L, Tan BC, Wong BH, et al. 2023. Blood-derived lysophospholipid sustains hepatic phospholipids and fat storage necessary for hepatoprotection in overnutrition. *The Journal of Clinical Investigation* 133:e171267
[46] van der Veen JN, Kennelly JP, Wan S, Vance JE, Vance DE, et al. 2017. The critical role of phosphatidylcholine and phosphatidylethanolamine metabolism in health and disease. *Biochimica et Biophysica Acta (BBA) - Biomembranes* 1859:1558–1572
[47] Jaafarinia A, Kafami B, Sahebnasagh A, Saghafi F. 2022. Evaluation of therapeutic effects of crocin in attenuating the progression of diabetic nephropathy: a preliminary randomized triple-blind placebo-controlled trial. *BMC Complementary Medicine and Therapies* 22:262
[48] Drygalski K. 2025. Pharmacological treatment of MASLD: contemporary treatment and future perspectives. *International Journal of Molecular Sciences* 26:6518
[49] Brisnovali NF, Haney C, Goedeke L. 2024. Rezdiffra™ (resmetirom): a THR-β agonist for non-alcoholic steatohepatitis. *Trends in Pharmacological Sciences* 45:1081–1082
[50] Zhang C, Wang J. 2025. Adverse events associated with obeticholic acid: a real-world, pharmacovigilance study. *Expert Opinion on Drug Safety* 10:1–9